ACS APPLIED NANO MATERIALS
Cite This: ACS Appl. Nano Mater. 2019, 2, 5149−5155
Article
www.acsanm.org

Color-Tunable All-Inorganic $CsPbBr_3$ Perovskites Nanoplatelet Films for Photovoltaic Devices

Mehmet Ozcan,[†] Sercan Ozen,[†] Gökhan Topcu,[‡] Mustafa M. Demir,[‡] and Hasan Sahin*[,†,§]

[†]Department of Photonics, Izmir Institute of Technology, 35430, Izmir, Turkey
[‡]Department of Materials Science and Engineering, Izmir Institute of Technology, 35430, Izmir, Turkey
[§]ICTP-ECAR Eurasian Center for Advanced Research, Izmir Institute of Technology, 35430, Izmir, Turkey

ABSTRACT: Herein, we demonstrate a novel coating approach to fabricate $CsPbBr_3$ perovskite nanoplatelet film with heat-free process via electrospraying from precursor solution. A detailed study is carried out to determine the effect of various parameters such as ligand concentration, electric field, flow rate, etc. on the optical properties. By controlling the volume ratios of the oleylamine (OAm) and oleic acid (OA), the coalescing and thickness of the resulting nanoplatelets can be readily tuned that results in control over emission in the range of 100 nm without any antisolvent crystallization or heating processes. The varying electrical field and flow rate was found as inefficient on the emission characteristics of the films. In addition, the crystal films were obtained under ambient conditions on the ITO coated glass surfaces as in the desired pattern. As a result, we demonstrated a facile and reproducible way of synthesizing and coating of $CsPbBr_3$ perovskite nanoplatelets which is suitable for large-scale production. In this method, the ability of tuning the degree of quantum confinement for perovskite nanoplatelets is promising approach for the one-step fabrication of crystal films that may enable the use in optoelectronics.

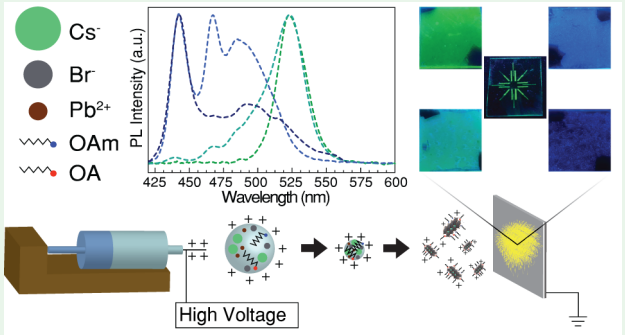

KEYWORDS: *coating, $CsPbBr_3$, electrospraying, nanoplatelet, perovskite, perovskite film*

I. INTRODUCTION

All-inorganic cesium lead halide perovskites (ILHPs) have attracted tremendous attention in recent years. Due to their extraordinary optical peculiarities, ILHPs are gaining wide variety of roles as strong contenders in optoelectronic research with tunable band gap, large absorption cross-section, long carrier lifetime, and high carrier mobility.[1−6] Therefore, the fabrication of ILHP nanostructures with controllable composition, morphology, dimensionality, and orientation has become important as the main focus, in order to employ the perovskites' superior properties in photovoltaics.[7]

Because of their applicability in photovoltaics, including solar cells and light-emitting diodes (LEDs), the fabrication methods of perovskite thin films with desired shape and size is crucial. For instance, the large crystal size or grain boundaries decrease the electroluminescence (EL) performance of perovskite light-emitting diodes (PeLEDs) because of trap states.[8−10] The probability for nonradiative recombination in large-sized crystals mostly increases, which results in a low EL efficiency for PeLEDs.[11,12] Similarly, PeLEDs performance suffers from trap state-induced nonradiative energy transfer, leading to low photoluminescence (PL), quantum yields (QY), and short PL lifetimes.[13] Therefore, attaining ultralow defective and impurity-free materials is necessary to achieve high performance for conventional semiconductors.[14]

In order to reduce the nonradiative energy transfer and obtain perovskites with high crystal quality, controllable (e.g., morphology and crystallinity) and low cost synthesis techniques have been examined by scientific area. To date, a number of synthesis methods have been reported such as ligand-mediated crystallization, hot injection,[1] and antisolvent crystallization.[15,16] In addition to their synthesis, the requirement of coating process to fabricate perovskite-based devices poses an additional step. In this context, single step strategies such as antisolvent vapor treatment, polymer additive assisted film growth, precursor solution composition optimization,[17−20] hand spray coating,[21,22] and electrospraying has been developed to simultaneously fabricate the crystal and its thin layer. Among these methods, electrospraying offers an opportunity to achieve high purity, size, and shape control and to lower the excessive usage of volatile chemical compounds.

Electrospraying is an all-purpose technique in which under an electric field between the tip and a grounded collector, fine liquid droplets are repelled from a sharp tip onto a metal or metal-supported substrate for coating.[23] Naphade et al. reported an approach for the synthesis of low-dimensional

Received: June 1, 2019
Accepted: July 17, 2019
Published: July 17, 2019

DOI: 10.1021/acsanm.9b01035
ACS Appl. Nano Mater. 2019, 2, 5149−5155

$MAPbX_3$-based perovskite colloidal nanostructures in a single step by combining antisolvent solvent extraction technique with the electrospraying process.[24] The handicap of this process is that the antisolvent bath in a metal electrode container is used as a collector instead of a solid substrate. Therefore, one can be required to perform some further steps such as centrifugation, dispersing, and spin-coating or drop-cast, etc. in order to apply perovskites on the desired substrate for device application. In another study, Hong et al. proposed a technique that enables uniform perovskite coatings on hot substrates by electrospray coating system.[25] However, heating the collector requires extra energy and increases the cost of fabrication.

In this study, we report a room temperature direct synthesis and coating approach of perovskite nanoplatelet film by using electrospray system. With a simple setup, this system can consistently provide stable conditions and a uniform coating process, which leads to the fabrication of nanoplatelets. Furthermore, the rate of coalescing of nanoplatelets can be easily controlled in the desired degree of quantum confinement by adjusting surfactant fraction and viability of this technique for lithography applications are also discussed.

II. RESULTS AND DISCUSSION

The solidified nanocrystals were grown on an ITO substrate by the electrospraying method. Spraying of the solution can be achieved only above particular electrical bias since the applied potential is required to overcome the surface tension of the precursor droplets. Eventually, the solution reaches to the needle head and directly wells out as a jet to grounded substrate, namely ITO (Figure 1(a) and (b)). The accelerated

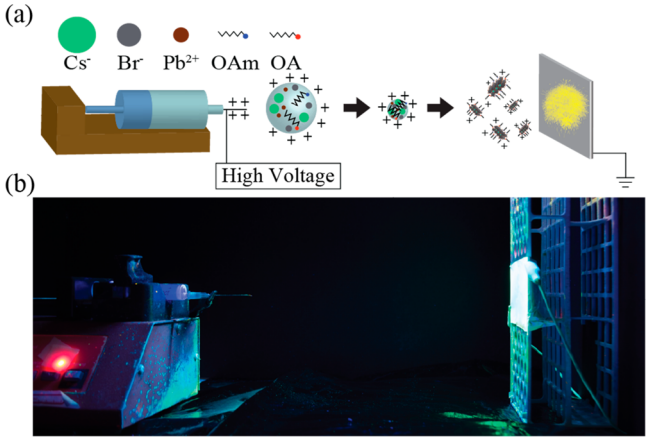

Figure 1. (a) Schematic representation and (b) photographic image of electrospraying setup.

droplets through the electric field transforms from liquid state into solid state forming crystals due to evaporation. Consequently, the crystals were deposit onto ITO when they reach the substrate. In this wise, the crystallization can be readily controlled by changing ligand fraction or electrospraying experimental parameters such as solvent ratio, applied voltage and flow rate. Huang et al. reported that the geometric packing of the varying amount of oleylamine who bonded to the $PbBr_4$ octahedra enables the control of morphologies from varying thicknesses nanoplatelets to nanoparticles.[26] In order to achieve full control over crystal geometry, in various amount of OAm was employed all of the electrospraying processes due to its ability of intercalation between the thin layers of $PbBr_6$ octahedra. Therefore, OAm intercalation can lead to isolation of 2D perovskite nanoplatelets. The effect of OAm was investigated in the presence of OA.

In order to observe the effect of OAm, various amount of OAm was mixed to the precursor solution having 500 μL of OA. The precursor solution was electrosprayed onto the ITO substrate under electric potential (20 kV). As a result of the processes, the perovskite films were obtained with a various optical properties. Appearance of the films under both daylight and UV light (254 nm) is presented in Figure 2(a). A long-range control on emission characteristics from green to dark blue is achieved as a function of OAm in the precursor solution. The images reveal that the lack of OAm leads to form nonemissive larger crystals showing intense orange color (first images from right). As the perovskite crystal grows, it becomes more defect tolerant.[35] Due to formation of highly defective crystals, emission lifetime increases which results in non-emissive behavior. Therefore, it is observed that the opacity of the films gradually decreases as OAm fraction increases. On the other hand, excessive amount of OAm causes lack of emission due to passivation of crystal growth. The optical properties (PL, absorption) of corresponding films are presented in Figure 2(b) and (c). By decreasing the amount of OAm, sharp absorption peak at 430 nm that is attributed to the thin nanoplatelets, gradually fades away (Figure 2(b)).[27,28] Moreover, it is also observed that according to the amount of intercalation agent (amount of OAm), the photoluminescence characteristics of the films distinctly varies. The use of OAm with 375 μL leads to sharp signals at 436 and 464 nm and broad ones at 482, 493, and 525 nm nm in PL spectrum. As the amount of OAm decreases, the weak signals start to emerge toward 525 nm and intensity of high energetical peaks decrease. The PLQY of the films varies between 30 and 40%. The behavior of relative intensities of PL peaks and absorption spectra hint about the thickening of the nanoplatelets by coalescing of nearby counterparts.[29−32] PL spectra suggest that the majority of PL intensities switch between high energetical (blue) and low energetical (green) regions by changing the OAm volume in the precursor solution.

The OAm molecules act as intercalation agent that binds to desired surface and creates a barrier against the coalescing of nanoplatelets. Hence, it results in 2D nanoplatelets and preservation of quantum confinement.[33,34] The experimental results point out that OAm has a dramatic effect on emission characteristics, namely quantum size effect, by probably mitigating crystal growth.

Further structural investigation was performed via X-ray diffraction (XRD) measurements, as shown in Figure 3. Since the crystal films are collected on ITO substrate, its diffraction pattern is barely recorded and presented in Figure 3(a). The 2θ reflections at 15° and 30° refer to (001) and (002) planes of $CsPbBr_3$ crystal structure, respectively, (JPDCS no. 01−075−0412) as seen in Figure 3(b) and (c). Therefore, the diffraction patterns of greenemitting and nonemissive films correspond to the cubic phase of $CsPbBr_3$ crystal structure. On the other hand, it is observed that these characteristic reflections are disappeared and the new 2θ reflections gradually emerge at 11.5°, 12.6°, and 25°, as the fraction of OAm increases (Figure 3(d) and (e)). These new peaks at small angles may hint about the presence of perovskite nanoplatelet.[34,36]

DOI: 10.1021/acsanm.9b01035
ACS Appl. Nano Mater. 2019, 2, 5149−5155

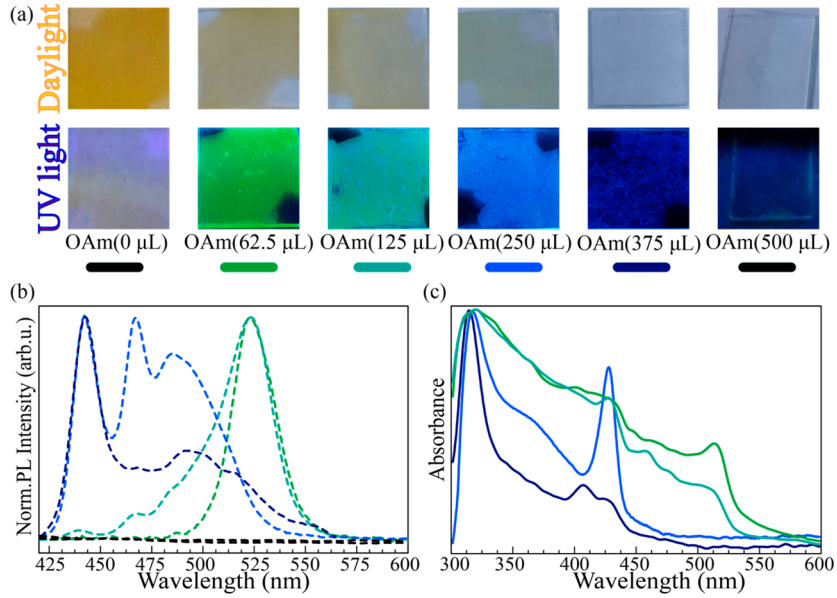

Figure 2. (a) Photographic image under daylight and under 254 nm UV light, (b) photoluminescence, and (c) absorption spectra of perovskite films according to the amount of OAm in the presence of oleic acid (500 μL).

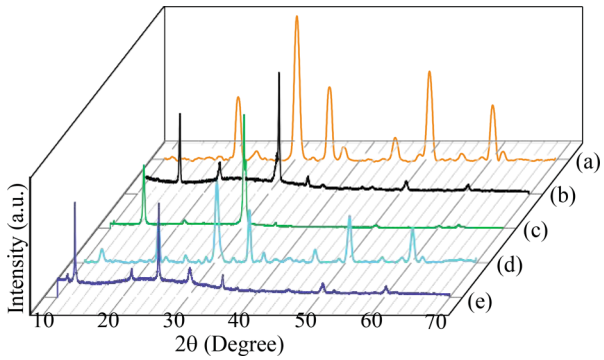

Figure 3. XRD diffractograms of (a) bare ITO substrate, (b) nonemissive, (c) green emitting, (d) cyan emitting, and (e) blue emitting perovskite films on ITO.

Additionally, thickness and morphological investigations of the perovskite films were done by surface and cross-section SEM images as seen in Figure 4(a) and (b). Perovskite film thickness distribution is obtained as approximately 2.53 μm from cross-section SEM image with a fwhm of 110 nm(Figure 4(c)). These results prove the homogeneity of perovskite film thickness and quality on ITO/glass substrate. For device applications, ability of homogeneously coating process is very crucial and electrospraying method promises a good quality perovskite films.

For further structural examination, layered morphology of the crystals was investigated using STEM for dominantly blue, cyan, and green emitting perovskite film as seen in Figure 5(a) and (b), respectively. STEM images were compared depending on the changing OAm fraction. Regional contrast differences are observed in the images, which indicate that the vertically stacked nanoplatelets vary in terms of thickness. Therefore, the stacking can influence the confinement, particularly. Note that the resulting perovskite films exhibit discrete emission peaks depending on the OAm fraction. In Figure 2(c), the energy difference between discrete PL maxima decreases as the layer thickness increases since the perovskite layer thickening causes a reduction in the degree of quantum confinement. On the other hand, the particle size distributions fluctuate between 200 and 500 nm for all cases. Since the size of the crystals seems to larger for the contribution of quantum confinement, it hints about the 2D structure of the materials. As a result, these agreements also support the peak assignment of the resulting perovskite films. In general, nanoplatelets tend to form bulk crystals that can be prevented by using intercalation agent, namely OAm. Nevertheless, the use of a moderate amount of OAm cannot completely stabilize the crystals so that the nanoplatelets thicken, however, they cannot align on

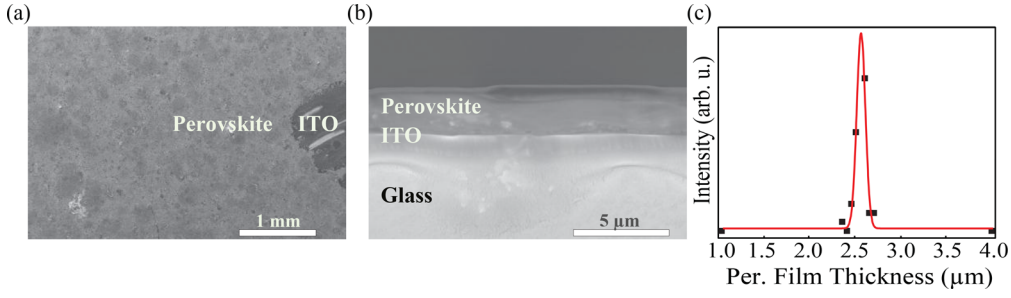

Figure 4. SEM images of (a) surface, (b) cross-section of the perovskite films, and (c) perovskite film thickness distribution on ITO/Glass substrate.

DOI: 10.1021/acsanm.9b01035
ACS Appl. Nano Mater. 2019, 2, 5149−5155

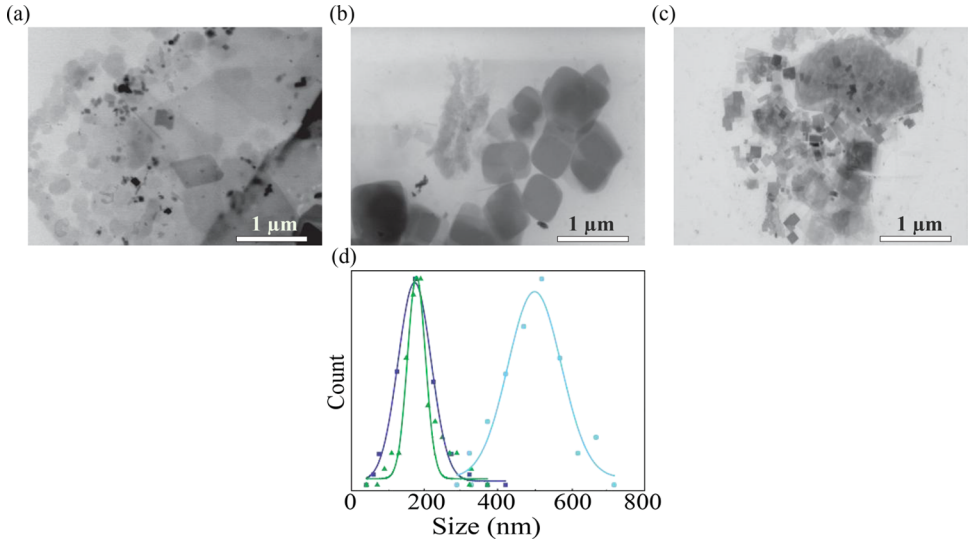

Figure 5. STEM images of (a) blue-, (b) cyan-, (c) green-emitting perovskite crystals, and (d) the particle size distributions.

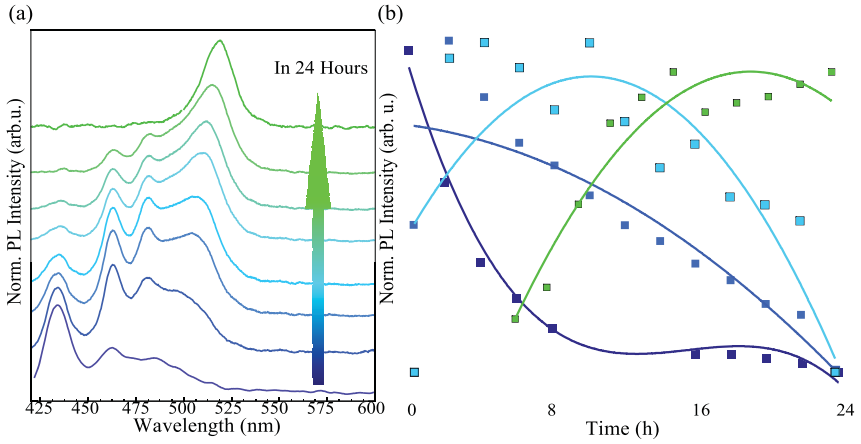

Figure 6. (a) Time dependent PL evolution of blue emitting perovskite film and (b) the time interval evolution of PL spectra for the signals appeared at 436, 464, 482, and 515 nm.

each other, perfectly. Hence, it results in nonhomogeneous confinement, which leads to a number of discrete PL energy levels.

Furthermore, photoluminescence evolution was monitored in time for blue emitting perovskite film and given as a function of time (Figure 6). It is observed that intense PL peak at 436 nm decreases in time and the relative intensities of 462, 480, and 515 nm PL peaks increase, respectively, in 24 h. This result indicates that the nanoplatelets are slowly getting thicker. For the thickening of the nanoplatelets in time, one can proposed that the detachment of OAm due to environmental conditions result in coalescence of the crystals. Since the decreasing OAm on the lateral surface leads to instability, the ionic character of the surfaces causes the integration of the individual nanoplatelets, therefore thickening.[37] On the other hand, it also proves that the presence of perovskite nanoplatelets which are isolated from each other.

Furthermore, optoelectronic properties of the perovskite films were studied by changing electrospraying parameters such as voltage, flow rate, and solvent (DMF) fraction in precursor. In Figure 7, the evolution of PL characteristics of 2D nanoplatelets is presented upon different parameters of electrospraying system with the 400 μL control precursor solution (OA-500 μL, OAm-250 μL).

In Figure 7(a) the PL spectra of the crystals that are obtained using different flow rates are presented. Varying the flow rate results in no change for PL peak positions. However, in the case of 0.25 mL/h flow, the change in PL peak intensity is observed. The relative PL shifts toward low energetic region. Note that the process time increases as the flow rate decreases. Therefore, the coating process takes 96, 24, and 16 min, respectively, by using the same amount of precursor solution. Hence, the origin of the red shift in the relative PL of 0.25 mL/h is the exposure of crystals to ambient conditions for a longer time. It can be concluded that the optical properties of the films are unchanged as a function of flow rate. On the other hand, in Figure 7(b), PL spectra of the resulting crystals are given for various potential differences. The potential difference controls the speed of electrosprayed droplets, therefore, evaporation rate of DMF. It is observed that the most of droplets are unable to lose their liquid phase to form nanocrystals, in the case of 10 and 15 kV. The evaporation of the droplets is finished on ITO, which leads to formation of relatively larger crystals. Therefore, the peak at 493 nm appears more intensive. As the potential difference increases to 20 kV,

DOI: 10.1021/acsanm.9b01035
ACS Appl. Nano Mater. 2019, 2, 5149−5155

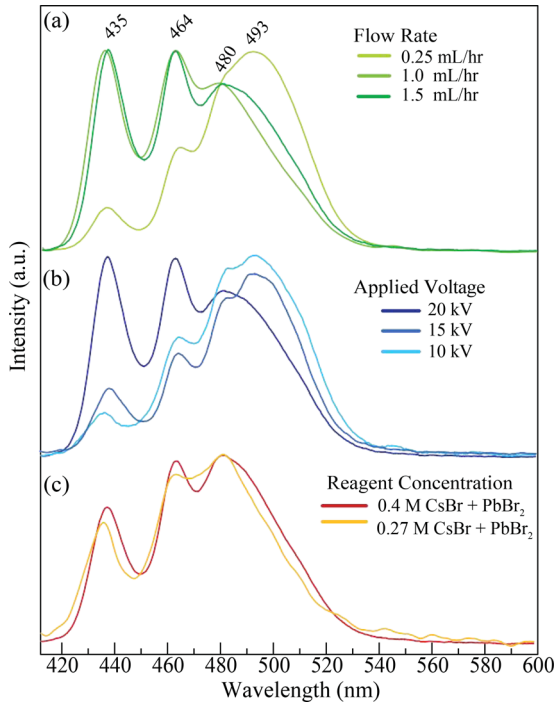

Figure 7. PL spectra of control sample with different (a) flow rate, (b) applied potential, and (c) reagent concentration.

the free-fly crystallization is achieved that results in more quantum confined perovskite film on the ITO. Furthermore, as seen in Figure 7(c), relative PL behavior is examined depending on the reagent concentration of precursor for normal (0.4 M CsBr + $PbBr_2$) and 33% lower one. Resulting films show no any significant PL peak shifts or change due to number of ions per droplet. Therefore, it is observed that electrospraying parameters and reagent concentration have no any effect on optoelectronic properties of perovskite nanoplatelets. However, it is achieved by only varying ligand ratios.

For the manufacturing of integrated optoelectronic devices without losing functionality of the material, large area patterning is a crucial process. Due to their unique properties, a numerous techniques are used to fabricate optoelectronic devices using perovskites have been given a great deal of attention. Patterning is a big challenge for mass-production applications with perovskites which are solution-based soft materials. To fabricate the film in exact shape and pattern, polyethylene terephthalate (PET) made logo mask, obtained by laser cutting, was used. The mask was placed on ITO coated glass, and patterned perovskite film was coated onto substrate via electrospraying. As seen in Figure 8, it is confirmed that the electrospraying method enables the direct patterning and synthesizing of perovskite films with tunable optoelectronic properties in minutes. Additionally, it minimizes the fabrication-induced loss of the device.

III. CONCLUSION

In a conclusion, one pot synthesis and coating of $CsPbBr_3$ nanoplatelets by electrospraying is investigated as a facile and low cost process. Without using antisolvent or heating for crystallization, simply prepared precursor solution was sprayed under electric field onto the ITO. It is found that the proposed method leads to formation of $CsPbBr_3$ nanoplatelets. By increasing the OAm fraction in precursor solution, the degree of quantum confinement of nanoplatelets goes up as OAm acts as intercalation agent between nanoplatelets. In addition, the great potential of electrospraying method for various applications was introduced by millimeter sized patterning. In summary, the electrospraying method offers an alternative and one-step route for the mass production of perovskite-based applications such as photodetectors, solar cells, light-emitting diodes, etc. with its low cost, facile, and fast perovskite film coating opportunities and enables a successful bridge between lab scale and industrial scale device fabrication with tunable degree of quantum confinement from a fundamental point of view. Last, but not least, this method may enable the formation of other phases of cesium lead halide perovskites and organic−inorganic hybrid perovskites.

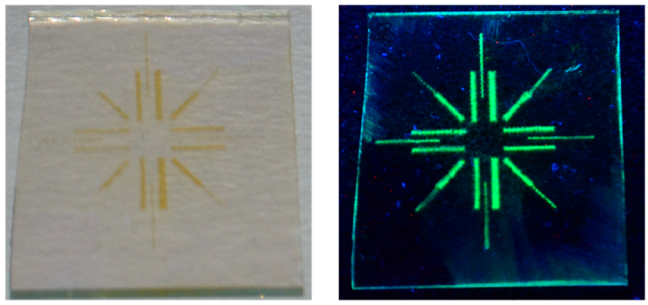

Figure 8. Patterned perovskite film on ITO, under daylight and UV light (254 nm).

IV. EXPERIMENTAL SECTION

Materials. Cesium Bromide (CsBr, 99.99%, Sigma-Aldrich), lead(II) bromide ($PbBr_2$, ≥98%, Sigma-Aldrich), oleic acid (OA, 90%, Alfa Aesar), oleylamine (OAm, 90%, Sigma- Aldrich), N,N-dimethylformamide (DMF, ≥99.9%, Tekkim) were purchased and used as received without any further purification.

Preparation of Precursor Solution. The precursor solution was prepared by following the method proposed by Li et al.[38] CsBr (0.4 M), $PbBr_2$ (0.4 M) and DMF (10 mL) are loaded into a 20 mL glass vial and mixed via magnetic stirrer. After full dissolution of the salts, desired amount of OA and OAm are added to the solution under vigorous stirring.

Fabrication of $CsPbBr_3$ Thin Films. An aliquot of the precursor solution (0.4 mL) was loaded into a plastic syringe with an inner diameter of 1.3 mm. For electrospraying by electric field between stainless-steel needle (21Gx1 1/2, Interlab) and ITO coated glass (Rs<10 Ω/sq., Teknoma), the electric voltage was applied from 10 to 20 kV by DC power supply (Gamma H. V. Research Ormand Beach, FL). The flow rate was controlled between 0.25 and 1.5 mL/h by a programmable syringe pump (SyringePump, NE-1000). The distance between the needle and ITO substrate was fixed to 16 cm.

Characterization. Optical characterizations including photoluminescence and absorption were obtained by USB2000+ Spectrometer (Ocean Optics Inc., Dunedin, FL, USA) via a premium fiber cable. The diffraction profile of the $CsPbBr_3$ structures was recorded with an X-ray diffractometer (XRD, XPert Pro, Philips, Eindhoven, The Netherlands). Scanning transmission electron microscopy (STEM; Quanta 250, FEI, Hillsboro, OR) was used to determine the morphology of crystals via STEM detectors. In the case of STEM characterization, the samples are dispersed in the hexane and the colloidal dispersion in hexane was drop-casted on Formvar reinforced copper grids and dried in a vacuum.

AUTHOR INFORMATION

Corresponding Author

*E-mail: hasansahin@iyte.edu.tr.

DOI: 10.1021/acsanm.9b01035
ACS Appl. Nano Mater. 2019, 2, 5149−5155

ORCID

Mustafa M. Demir: 0000-0003-1309-3990

Hasan Sahin: 0000-0002-6189-6707

Notes

The authors declare no competing financial interest.

■ ACKNOWLEDGMENTS

H.S Acknowledges financial support from the TUBITAK under the project number 117F095. Characterization techniques (STEM and XRD) were performed by Izmir Institute of Technology, Center for Materials Research.

■ REFERENCES

(1) Protesescu, L.; Yakunin, S.; Bodnarchuk, M. I.; Krieg, F.; Caputo, R.; Hendon, C. H.; Yang, R. X.; Walsh, A.; Kovalenko, M. V. Nanocrystals of Cesium Lead Halide Perovskites (CsPbX3, X = Cl, Br, and I): Novel Optoelectronic Materials Showing Bright Emission with Wide Color Gamut. *Nano Lett.* **2015**, *15*, 3692−3696.

(2) Akkerman, Q. A.; D'Innocenzo, V.; Accornero, S.; Scarpellini, A.; Petrozza, A.; Prato, M.; Manna, L. Tuning the optical properties of cesium lead halide perovskite nanocrystals by anion exchange reactions. *J. Am. Chem. Soc.* **2015**, *137*, 10276−10281.

(3) Makarov, N. S.; Guo, S.; Isaienko, O.; Liu, W.; Robel, I.; Klimov, V. I. Spectral and dynamical properties of single excitons, biexcitons, and trions in cesium-lead-halide perovskite quantum dots. *Nano Lett.* **2016**, *16*, 2349−2362.

(4) Stranks, S. D.; Eperon, G. E.; Grancini, G.; Menelaou, C.; Alcocer, M. J. P.; Leijtens, T.; Herz, L. M.; Petrozza, A.; Snaith, H. J. Electron-hole diffusion lengths exceeding 1 micrometer in an organometal trihalide perovskite absorber. *Science* **2013**, *342*, 341−344.

(5) Li, C.; Zang, Z.; Chen, W.; Hu, Z.; Tang, X.; Hu, W.; Sun, K.; Liu, X.; Chen, W. Highly pure green light emission of perovskite CsPbBr3 quantum dots and their application for green light-emitting diodes. *Opt. Express* **2016**, *24*, 15071−15078.

(6) Yan, D.; Shi, T.; Zang, Z.; Zhou, T.; Liu, Z.; Zhang, Z.; Du, J.; Leng, Y.; Tang, X. Ultrastable CsPbBr3 Perovskite Quantum Dot and Their Enhanced Amplified Spontaneous Emission by Surface Ligand Modification. *Small* **2019**, *15*, 1901173.

(7) Han, C.; Li, C.; Zang, Z.; Wang, M.; Sun, K.; Tang, X.; Du, J. Tunable luminescent CsPb2Br5 nanoplatelets: applications in light-emitting diodes and photodetectors. *Photonics Res.* **2017**, *5*, 473−480.

(8) Cho, H.; Wolf, C.; Kim, J. S.; Yun, H. J.; Bae, J. S.; Kim, H.; Heo, J.-M.; Ahn, S.; Lee, T.-W. High-Efficiency Solution-Processed Inorganic Metal Halide Perovskite Light-Emitting Diodes. *Adv. Mater.* **2017**, *29*, 1700579.

(9) Wei, Z.; Perumal, A.; Su, R.; Sushant, S.; Xing, J.; Zhang, Q.; Tan, S. T.; Demir, H. V.; Xiong, Q. Solution-processed highly bright and durable cesium lead halide perovskite light-emitting diodes. *Nanoscale* **2016**, *8*, 18021−18026.

(10) Pan, J.; Quan, L. N.; Zhao, Y.; Peng, W.; Murali, B.; Sarmah, S. P.; Yuan, M.; Sinatra, L.; Alyami, N. M.; Liu, J.; Yassitepe, E.; Yang, Z.; Voznyy, O.; Comin, R.; Hedhili, M. N.; Mohammed, O. F.; Lu, Z. H.; Kim, D. H.; Sargent, E. H.; Bakr, O. M. Highly Efficient Perovskite-Quantum-Dot Light-Emitting Diodes by Surface Engineering. *Adv. Mater.* **2016**, *28*, 8718−8725.

(11) Kim, Y.-H.; Cho, H.; Lee, T.-W. Metal halide perovskite light emitters. *Proc. Natl. Acad. Sci. U. S. A.* **2016**, *113*, 11694−11702.

(12) Cho, H.; Jeong, S.-H.; Park, M.-H.; Kim, Y.-H.; Wolf, C.; Lee, C.-L.; Heo, J. H.; Sadhanala, A.; Myoung, N.; Yoo, S.; Im, S. H.; Friend, R. H.; Lee, T.-W. Overcoming the electrolumines- cence efficiency limitations of perovskite light-emitting diodes. *Science* **2015**, *350*, 1222−1225.

(13) Chen, Q.; Zhou, H.; Song, T.-B.; Luo, S.; Hong, Z.; Duan, H.-S.; Dou, L.; Liu, Y.; Yang, Y. Controllable self-induced passivation of hybrid lead iodide perovskites toward high performance solar cells. *Nano Lett.* **2014**, *14*, 4158−4163.

(14) Brandt, R. E.; Stevanović, V.; Ginley, D. S.; Buonassisi, T. Identifying defect-tolerant semi- conductors with high minority-carrier lifetimes: beyond hybrid lead halide perovskites. *MRS Commun.* **2015**, *5*, 265−275.

(15) Schmidt, L. C.; Pertegás, A.; González-Carrero, S.; Malinkiewicz, O.; Agouram, S.; Espallargas, G. M.; Bolink, H. J.; Galian, R. E.; Peérez-Prieto, J. Nontemplate Synthesis of CH3NH3PbBr3 Perovskite Nanoparticles. *J. Am. Chem. Soc.* **2014**, *36*, 850−853.

(16) Zhang, F.; Zhong, H.; Chen, C.; Wu, X.-G.; Hu, X.; Huang, H.; Han, J.; Zou, B.; Dong, Y. Brightly Luminescent and Color-Tunable Colloidal CH3NH3PbX3 (X = Br, I, Cl) Quantum Dots: Potential Alternatives for Display Technology. *ACS Nano* **2015**, *9*, 4533−4542.

(17) Zhang, L.; Yang, X.; Jiang, Q.; Wang, P.; Yin, Z.; Zhang, X.; Tan, H.; Yang, Y. M.; Wei, M.; Sutherland, B. R.; Sargent, E. H.; You, J. Ultra-bright and highly efficient inorganic based perovskite light-emitting diodes. *Nat. Commun.* **2017**, *8*, 15640.

(18) Ban, M.; Zou, Y.; Rivett, J. P. H.; Yang, Y.; Thomas, T. H.; Tan, Y.; Song, T.; Gao, X.; Cred-Ington, D.; Deschler, F.; Sirringhaus, H.; Sun, B. Solution-processed perovskite light emitting diodes with efficiency exceeding 15% through additive-controlled nanostructure tailoring. *Nat. Commun.* **2018**, *9*, 3892.

(19) Yuan, S.; Wang, Z.-K.; Zhuo, M.-P.; Tian, Q.-S.; Jin, Y.; Liao, L.-S. Self-Assembled High Quality CsPbBr3 Quantum Dot Films toward Highly Efficient Light-Emitting Diodes. *ACS Nano* **2018**, *12*, 9541−9548.

(20) Wu, C.; Zou, Y.; Wu, T.; Ban, M.; Pecunia, V.; Han, Y.; Liu, Q.; Song, T.; Duhm, S.; Sun, B. Improved Performance and Stability of All-Inorganic Perovskite Light-Emitting Diodes by Antisolvent Vapor Treatment. *Adv. Funct. Mater.* **2017**, *27*, 1700338.

(21) Gamliel, S.; Dymshits, A.; Aharon, S.; Terkieltaub, E.; Etgar, L. J. Micrometer sized perovskite crystals in planar hole conductor free solar cells. *J. Phys. Chem. C* **2015**, *119*, 19722−19728.

(22) Ramesh, M.; Boopathi, K. M.; Huang, T.-Y.; Huang, Y.-C.; Tsao, C.-S.; Chu, C.-W. Using an airbrush pen for layer-by-layer growth of continuous perovskite thin films for hybrid solar cells. *ACS Appl. Mater. Interfaces* **2015**, *7*, 2359−2366.

(23) Kumar, P. S.; Sundaramurthy, J.; Sundarrajan, S.; Babu, V. J.; Singh, G.; Allakhverdiev, S. I.; Ramakrishna, S. Hierarchical electrospun nanofibers for energy harvesting, production and environmental remediation. *Energy Environ. Sci.* **2014**, *7*, 3192−3222.

(24) Naphade, R.; Nagane, S.; Shanker, G. S.; Fernandes, R.; Kothari, D.; Zhou, Y.; Padture, N. P.; Ogale, S. Hybrid Perovskite Quantum Nanostructures Synthesized by Electrospray Antisolvent-Solvent Extraction and Intercalation. *ACS Appl. Mater. Interfaces* **2016**, *8*, 854−861.

(25) Hong, S. C.; Lee, G.; Ha, K.; Yoon, J.; Ahn, N.; Cho, W.; Park, M.; Choi, M. Precise mor-phology control and continuous fabrication of perovskite solar cells using droplet-controllable electrospray coating system. *ACS Appl. Mater. Interfaces* **2017**, *9*, 7879−7884.

(26) Huang, J.; Wu, Y. H.; Zhu, Z. G.; Shih, W. Y.; Shih, W. H. Control of oleylamine to perovskite ratio in synthesis of MAPbBr3 nanoparticles. *Chem. Phys. Lett.* **2018**, *702*, 21−25.

(27) Nasilowski, M.; Mahler, B.; Lhuillier, E.; Ithurria, S.; Dubertret, B. Two-dimensional colloidal nanocrystals. *Chem. Rev.* **2016**, *116*, 10934−10982.

(28) Hong, X.; Ishihara, T.; Nurmikko, A. V. Dielectric confinement effect on excitons in PbI4-based layered semiconductors. *Phys. Rev. B: Condens. Matter Mater. Phys.* **1992**, *45*, 6961.

(29) Weidman, M. C.; Seitz, M.; Stranks, S. D.; Tisdale, W. A. Highly tunable colloidal perovskite nanoplatelets through variable cation, metal, and halide composition. *ACS Nano* **2016**, *10*, 7830−7839.

(30) Shamsi, J.; Dang, Z.; Bianchini, P.; Canale, C.; Di Stasio, F.; Brescia, R.; Prato, M.; Manna, L. Colloidal Synthesis of Quantum Confined Single Crystal CsPbBr3 Nanosheets with Lateral Size Control up to the Micrometer Range. *J. Am. Chem. Soc.* **2016**, *138*, 7240−7243.

DOI: 10.1021/acsanm.9b01035
ACS Appl. Nano Mater. 2019, 2, 5149−5155

(31) Tong, Y.; Bladt, E.; Aygüler, M. F.; Manzi, A.; Milowska, K. Z.; Hintermayr, V. A.; Docampo, P.; Bals, S.; Urban, A. S.; Polavarapu, L.; Feldmann, J. Highly Luminescent Cesium Lead Halide Perovskite Nanocrystals with Tunable Composition and Thickness by Ultrasonication. *Angew. Chem., Int. Ed.* **2016**, *55*, 13887−13892.
(32) Yuan, Z.; Shu, Y.; Xin, Y.; Ma, B. Highly luminescent nanoscale quasi-2D layered lead bromide perovskites with tunable emissions. *Chem. Commun.* **2016**, *52*, 3887−3890.
(33) Sichert, J. A.; Tong, Y.; Mutz, N.; Vollmer, M.; Fischer, S.; Milowska, K. Z.; Cortadella, R. G.; Nickel, B.; Cardenas-Daw, C.; Stolarczyk, J. K.; Urban, A. S.; Feldmann, J. Quantum Size Effect in Organometal Halide Perovskite Nanoplatelets. *Nano Lett.* **2015**, *15*, 6521−6527.
(34) Yang, X.; Zhang, X.; Deng, J.; Chu, Z.; Jiang, Q.; Meng, J.; Wang, P.; Zhang, L.; Yin, Z.; You, J. Efficient green light-emitting diodes based on quasi-two-dimensional composition and phase engineered perovskite with surface passivation. *Nat. Commun.* **2018**, *9*, 570.
(35) Kang, J.; Wang, L. W. High Defect Tolerance in Lead Halide Perovskite CsPbBr3. *J. Phys. Chem. Lett.* **2017**, *8*, 489−493.
(36) Bekenstein, Y.; Koscher, B. A.; Eaton, S. W.; Yang, P.; Alivisatos, A. P. Highly luminescent colloidal nanoplates of perovskite cesium lead halide and their oriented assemblies. *J. Am. Chem. Soc.* **2015**, *137*, 16008−16011.
(37) Akbali, B.; Topcu, G.; Guner, T.; Ozcan, M.; Demir, M. M.; Sahin, H. CsPbBr3 perovskites: Theoretical and experimental investigation on water-assisted transition from nanowire formation to degradation. *Phys. Rev. Matt.* **2018**, *2*, 034601.
(38) Li, X.; Wu, Y.; Zhang, S.; Cai, B.; Gu, Y.; Song, J.; Zeng, H. CsPbX3 Quantum Dots for Light-ing and Displays: RoomTemperature Synthesis, Photoluminescence Superiorities, Underlying Origins and White Light-Emitting Diodes. *Adv. Funct. Mater.* **2016**, *26*, 2435−2445.

DOI: 10.1021/acsanm.9b01035
ACS Appl. Nano Mater. 2019, 2, 5149−5155